PCCP

ARTICLE TYPE

Cite this: DOI: 00.0000/xxxxxxxxxx

Effect of mild nanoscopic confinement on the dynamics of ionic liquids

Daria Noferini,[a] Olaf Holderer,[a] and Henrich Frielinghaus[a]

Received Date
Accepted Date

DOI: 00.0000/xxxxxxxxxx

Ionic liquids are molten salts without additional solvent and are discussed as innovative solvents and electrolytes in chemical processing and electrochemistry. A thorough microscopic understanding of the structure and ionic transport processes is essential for tailored applications. Here, we study the influence of "mild" nanoscopic confinement on the structure and diffusion properties of an ionic liquid, 1-Ethyl-3-methylimidazolium acetate, with scattering techniques. The structure is analyzed with x-ray diffraction, while neutron backscattering spectroscopy is employed for the study of the diffusion processes in these systems. Interpreting the diffusion processes in terms of a jump-diffusion model allowed to deduce confinement effects on the jump length and residence time, both increased at elevated temperatures in confinement. The applied "mild" confinement, which leaves room for 10-25 times the domain spacing, allows to observe in much detail how the onset of domain distortion decelerates the dynamics.

1 Introduction

Ionic liquids (IL) attracted much interest as innovative solvents used in synthesis [1], electrochemistry acting for examples as electrolyte [2] and are also of large interest for fundamental research in chemistry and physics [3,4]. The ionic transport within an ionic liquid is one of the prominent questions in terms of applicability as a solvent in electrochemical energy converters (fuel cells, electrolyzers) [5,6]. The structure of ionic liquids has been studied with scattering techniques such as x-ray reflectivity [7] or small angle neutron scattering (SANS) [8]. Interestingly, several orders of diffraction peaks are observed [9,10] where the molecule spacing scales with the molecule size, and the surface tension is reduced [11]. Molecular Dynamics simulations have been employed to calculate physical properties of an ionic liquid such as diffusion constants, radial distribution functions and confinement effects [12–14]. Very often a high confinement down to a very few molecule layers was considered [14,15]. Experimentally, the ion transport within an ionic liquid has been addressed with PFG-NMR and quasielastic neutron scattering (QENS) for an ionic liquid exhibiting nano structures [16], whereas an increased ionic mobility has been reported for 1D-confinement of an ionic liquid inside carbon nanotubes [17,18]. In extreme (bidisperse) pore confinement [19] of few and sub nanometers the alternating domain structure seems to be widely suppressed, while the diffusion is slowed down. A similar study with bidisperse hierarchical pores found a very complicated scenario with "highways" for ion transport [20]. However, phase boundaries seem to be rather unaffected by pore confinement [21].

In this work we present results on the structure and dynamics of ionic liquid 1-Ethyl-3-methylimidazolium acetate (hereafter indicated as EmimAc) [22] in the bulk state and confined in porous glasses with different pore diameter. The here studied pore sizes range from 10 to 25 times the molecule pair size (i.e. repeat distance), which is considerably larger than in many other studies focusing on a few molecule layers such as in carbon nanotubes [17,18] or nanometer gaps in simulations [14,15]. We thus term this confinement as "mild", since the ionic liquid still has considerable space to arrange itself and only a rather small fraction is actually in direct contact with the glass surface. The influence of the size of confinement on the structure and details of the diffusion process of the ions are studied by X-ray diffraction and QENS.

2 Experimental

The IL 1-ethyl-3-methylimidazolium acetate (EmimAc, 97% purity) was purchased from Sigma-Alrdich and used as received. The porous glass Varapor-100 (noted as VP) and AGC-40 (noted as AGC) were purchased from the company Advanced Glass and Ceramics (www.porousglass.com) with a diameter of 14 mm and 0.5 mm thickness. The chemical compositions of the glasses were provided as VP: better than 99% SiO_2; AGC: 95% SiO_2, 5% B_2O_3. Natural glass surfaces [23] have a surface charge of -0.77 C/m^2 due to the dissociation of the silanol groups. However the Debye-Hückel model would predict a Debye length of sub-Ångström and so all surface charges are shielded by the first layer of cations. For reusing the glass, the pieces were kept overnight in methanol and

[a] Forschungszentrum Jülich GmbH, Jülich Centre for Neutron Science (JCNS) at Heinz Maier-Leibnitz Zentrum (MLZ), Garching, Germany. E-mail: o.holderer@fz-juelich.de

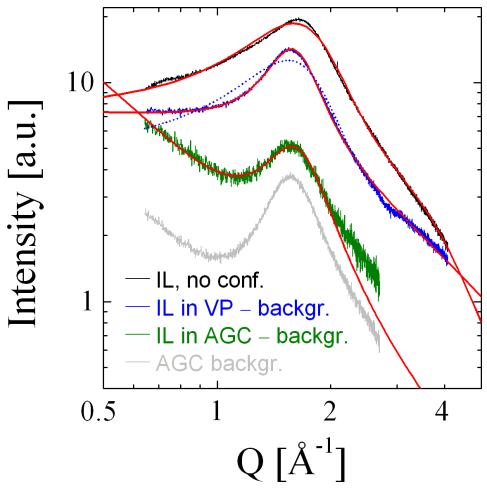

Fig. 1 X-ray diffraction patterns of the IL without confinement, in VP and AGC with model fits (red & dotted blue) as discussed in the main text.

dried in vacuum. The glasses were filled with a meniscus of IL on top at 100 °C under high vacuum overnight, and paperdried after the application. Specifications are listed in Table 1. The discrepancy in the nominal size vs. pore size distribution lies in the number average vs. volume weighted distribution. From the volume weighted distributions the overlap of the two glasses is well beyond the 1σ-limit and thus the glasses can be considered to be different. The specific surfaces of the two glasses are 116 and 215 m^2/g (VP and AGC) according to the producer.

X-ray diffraction (XRD) was performed on single glass samples and the pure IL on a Bruker D2 Phaser with a copper Kα source (λ=1.541 Å, operated at 30 kV, 10 mA). The incident beam was collimated to 0.1° divergence. The shading characteristics of the beam stop from the rather flat scattering of the neat IL have been used to correct the scattering at smallest angles. The pure glass scattered considerably less than the IL. For the IL confined in AGC, the background substracted scattering from the IL and the scattering of the empty AGC glass are presented in Figure 1. For neutron experiments, the bulk IL sample was placed in a cylindrical cell with annular geometry and Al walls with a thickness of 0.5 mm. The inner diameter of the external cylinder of 24 mm left a gap of 0.1 mm. For the confined samples, three glass disks were vertically arranged between two Al plates of 0.5 mm thickness that were sealed by laser-welding.

Table 1 Specifications of the pore size and porosity for the two porous glasses.

Glass	nominal pore diam.	pore diam. distr.	porosity
VP	98 Å	135±44 Å	40%
AGC	37 Å	50±17 Å	31%

The QENS measurements were conducted at the high-resolution backscattering spectrometer SPHERES at the Heinz Maier-Leibnitz Zentrum (MLZ) in Garching, Germany[24]. The instrument is operated with an incident wavelength of 6.27 Å and Si(111) unpolished analyzers, providing a resolution of *ca* 0.66 μeV and Q-range of *ca* 0.2–1.8 Å^{-1}. By moving the Doppler-monochromator at 4.7 m/s, a dynamical range of approx. ±31 μeV was obtained. For the measurements of the confined IL, the Al plates were oriented at 45° in transmission. VP disks with no absorbed IL and arranged in the same geometry and Al plates were measured for background subtraction of the confined IL. In the case of the measurements in AGC, the signal was re-scaled according to transmission ratios of VP and AGC. For the bulk measurements, an empty cell with the same annular cylinder geometry was measured and subtracted. Spectra were acquired at 3, 280, 320 and 373 K and analysed in the Q-range 0.6–1.4 Å^{-1}, where signal-to-noise and energy resolution are the highest and influence from the structural peaks are minor. The low-T measurements, after empty cell subtraction, were used as resolution functions $R(Q,\hbar\omega)$ in the data analysis and for detector normalisation. This approach is justified as the signal is dominated by the incoherent scattering of the hydrogen atoms and all dynamics are frozen out at the base temperature. For the bulk sample, the change of intensity in the elastic channel at $\hbar\omega = 0$ as function of the temperature (elastic fixed window scan; EFWS) was also examined, in the range 3−−373 K upon heating, with a heating rate of 0.7 K/min. Data reduction and corrections were carried out using the software SLAW[25] and LAMP[26], whereas the software LAMP and MATLAB were used for the fitting procedures.

3 Results and Discussion

The structure of the IL with and without confinement was determined using XRD (Fig. 1). The pure glass samples display significantly less scattering compared with loaded samples. The case of AGC is shown in Fig.1. The glass exhibits a characteristic SiO_2 peak above 1 Å^{-1}, which is still lower than the peak of the IL confined in AGC, where the glass scattering has been subtracted. All spectra displayed a clear correlation peak connected to the repeating distance of the IL. The neat IL was described by a microemulsion scattering function[27,28] because the alternating structure of anions and cations resembles that of oil and water and the IL often remains not aligned, i.e. disordered on macroscopic length scales:

$$I(Q) = \left(\frac{A}{(k_0^2+\xi^{-2})^2 - 2(k_0^2-\xi^{-2})Q^2 + Q^4} + B\,\frac{\mathrm{erf}^{12}(1.06QR_g/\sqrt{6})}{Q^4} \right) \exp(-\sigma^2 Q^2) \qquad (1)$$

with amplitudes A, and B, a wave vector for the repeat distance k_0, a correlation length ξ, a domain size gyration radius R_g, and a domain roughness σ. This scattering function does not originate from a diverging correlation function of the kind $\exp(-\xi r)\sin(k_0 r+\phi)/(k_0 r)$ in real space[7,8] with an non-zero phase shift ϕ. This non-zero phase shift was introduced to account for the dissymmetry of the correlation peak. For the here suggested function the dissymmetry is generated by the term containing the error function. It adds excess domain surface with the amplitude B to the Teubner-Strey expression with amplitude A. While the Teubner-Strey[27] expression results from a free energy Landau expansion at low Q, the excess surface needs to be

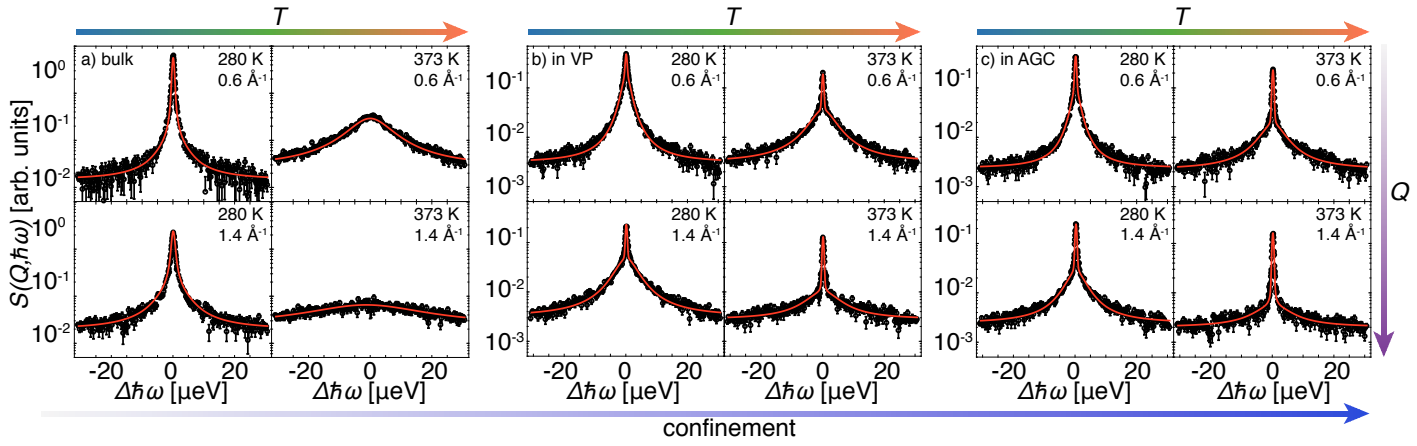

Fig. 2 Dynamic structure factor $S(Q,\hbar\omega,T)$ for a) EmimAc bulk, b) EmimAc in VP and c) EmimAc in AGC. For each sample, spectra at Q=0.6 (top) and 1.4 Å^{-1} (bottom) and T= 280 (left) and 373 K (right) are displayed. Red solid lines represent fits of the signal (see text). Data points are displayed as rebinned in energy, for clarity.

added explicitly. These thoughts hold well for microemulsions with approx. 10 nanometer domain sizes, and seem to apply for the current system as well. The ordered domains with random orientation are described by two Lorentzians[29]:

$$I(Q) = \frac{C_1}{1+\xi^2(Q-k_0)^2} + \frac{C_0}{1+\xi_0^2 Q^2} \quad (2)$$

again, with amplitudes C_0 and C_1, two correlation lengths ξ_0 and ξ. The domain wave vector is k_0. All fitting parameters are listed in Table 2. In Fig. 1 we explicitly display the mismatching microemulsion approach for the VP-sample by the dotted blue line. For the ordered systems, we directly see the strong increase of the correlation length ξ with confinement that goes along with the change of the model for bicontinuous vs. lamellar structures. The slight decrease of k_0 is statistically relevant and underlines the higher degree of order, possibly due to aligned or oriented molecules. Apart from the structural parameters, the extrapolated forward scattering $I(Q\to 0)$ is clearly higher for the AGC system, even though the scales of intensity are not fully comparable. Thus, the osmotic compressibility is higher for AGC[30], meaning that fluctuations of the stoichiometry are facilitated here.

Table 2 Structural parameters for describing the XRD scattering patterns according to eqs. 1 and 2. The error bars of the correlation peak parameters (k_0, ξ) are better than 1%, 1.6% for R_g, and 2.6% and 10% for ξ_0 for VP and AGC. σ was set fixed. Amplitude ratios are better that 1%.

Sample	k_0 [Å^{-1}]	ξ [Å]	3rd par.	4th par.	A/B, C_0/C_1
neat IL	1.70	1.62	$R_g = 0.95$ Å	$\sigma = 0.1$ Å	0.145
VP	1.58	3.25	$\xi_0 = 0.50$ Å	–	0.701
AGC	1.60	2.73	$\xi_0 = 3.93$ Å	–	12.0

In Fig. 2 we present selected spectra of the measured dynamic structure factor $S(Q,\hbar\omega,T)$. The signal becomes generally broader with increasing Q and T, suggesting thermally activated diffusion. Differences induced by the confinement can be also noticed, in particular a reduced influence of the temperature compared with the bulk sample.

A parametrization of the data is carried out with the following equation:

$$S(Q,\hbar\omega) = K\exp\left(\frac{-\langle u^2\rangle Q^2}{3}\right)[A_0(Q)\delta(\hbar\omega) + A_1(Q)L_1(Q,\hbar\omega)] \otimes R(Q,\hbar\omega) + b(Q) \quad (3)$$

where K is a normalisation constant, $\langle u^2\rangle$ is the vibrational mean square displacement, L_1 is a nornalised Lorentzian function multiplied by its weight A_1, and $b(Q)$ is a a flat, energy-independent, background. The elastic component, $A_0\delta(\hbar\omega)$, present in all spectra of the confined ionic liquid, indicates slow dynamics which cannot be resolved within the resolution of SPHERES. The bulk IL at elevated temperatures is a pure liquid sample and has no elastic component, so $A_0 = 0$ in this case. The bulk sample at 280 K showed an additional fast dynamics, making necessary the use of a second broad Lorentzian component in the fit. In Equation 3 the single Lorentzian is therefore replaced by $A_1(Q)L_1(Q,\hbar\omega) + (1-A_1(Q))L_2(Q,\hbar\omega)$, where the width of the Loretzian function L_2 is the sum of the widht of L_1 and the width of a localised component. Such a localised component likely becomes too fast, and thus too broad to be distinguished from the background, as the temperature increases. Interestingly, it is not observable in the confined samples at the same temperature. $A_0(Q)$ and $A_1(Q)$ (and $A_2(Q)$ if applicable) are normalised so that their sum is equal to 1 for each spectrum. In this context we note that in order to describe the complex dynamics of ILs, some groups have previously employed stretched exponential functions.[31–33] Our use of single Lorentzian components does not necessarily mean a Debye nature of the here investigated processes. Within the present experimental conditions such an approach, previously used in QENS studies on similar materials,[16,18,34–38] allows us to reduce complexity while sufficiently approximate the data, with the aim of obtaining qualitative information about the dynamics to compare the different samples and highlight the possible influence of the confinement.

We focus now on the component described by L_1. The Q-

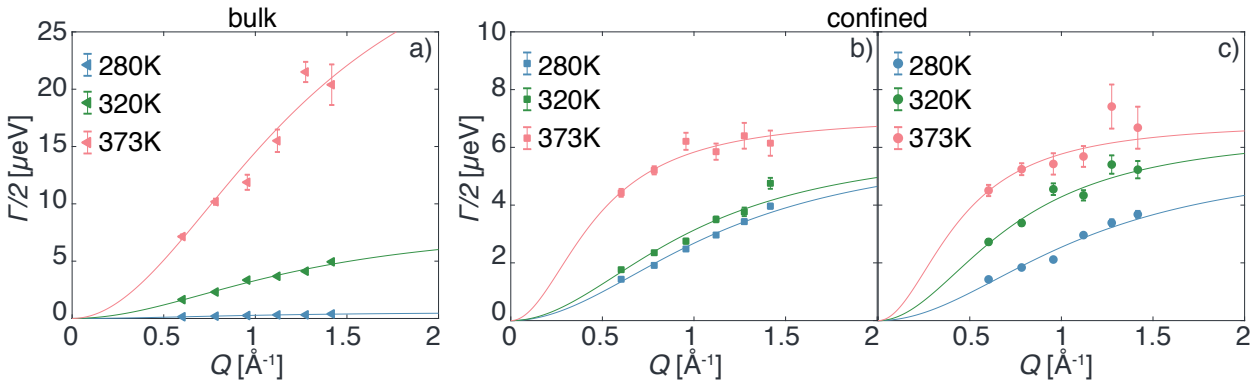

Fig. 3 Q-dependence of the widths of the quasielastic Lorentzian components for a) bulk EmimAc, b) EmimAc confined in VP, and c) EmimAc confined in AGC. Solid lines represent fits according to the SSM, Eq. 5.

dependence of the half width at half maximum of L_1, $\frac{\Gamma_1}{2}(Q)$, is shown in Figure 3 and clearly identifies the dynamics described by A_1L_1 as diffusive[39]. In particular it is well described by the jump diffusion model proposed by Singwi and Sjölander (SSM)[40], represented by the solid lines in Figure 3. Such a model was previously applied to describe dynamics in similar systems[16,18,20,34–38] and it assumes a diffusive motion *via* successive jumps spaced out by rests in a given site for a residence time τ. The jump distance $\rho(r)$ is exponentially distributed,

$$\rho(r) = \frac{r}{r_0^2}\exp\left(-\frac{r}{r_0}\right). \tag{4}$$

The Q-dependent quasielastic broadening is thus described as

$$\frac{\Gamma}{2}(Q) = \frac{\hbar}{6\tau}\frac{Q^2l^2}{\frac{Q^2l^2}{6}+1}, \tag{5}$$

where l^2 is the mean square jump length, which is equal to $\int_0^\infty r^2\rho(r)dr = 6r_0^2$.

The average jump lengths l and residence times τ as obtained from the fits according to Eq. 5 are presented in Figure 4 a) and b), respectively. In c), we report the Arrhenius plots of the diffusion coefficients, calculated as $D = \frac{l^2}{6\tau}$. The residence time decreases with increasing temperature and ranges for the bulk from 1.1(2) to 0.017(9) ns. The τ-values in the confined systems seem to be less influenced by the temperatures and ranges from 0.11(2) to 0.093(8) ns in VP and from 0.12(3) to 0.10(2) ns in AGC. Jump lengths are in the order of 1-2 Å, with different behaviour as a function of the temperature for bulk and confined systems. Values are again quite similar for the two confined systems, in the range 0.9-2.2 Å. In the bulk sample, the jump length is constant with temperature within the error bars and ranges from 0.9(2) to 0.8(3) Å.

Overall, the effect of confinement is therefore more evident in the extreme temperatures investigated here. At 280 K, the dynamics is much slower in the bulk sample: localised motions, too fast in the other samples and at higher temperatures, are here slow enough to enter into the dynamical range of SPHERES, whereas the diffusion described by A_1L_1 is at the edge of the experimental resolution and thus difficult to separate from it. At 373 K, the bulk shows a much shorter l but also much shorter τ with respect to the confined systems. As an effect, diffusion coefficients are very similar, around 6-9 $\times 10^{-7}$ cm^2/s.

The activation energies derived by fitting $D(T)$ according to Arrhenius law (solid lines in Figure 4 c)) are in the range of 0.2-0.3 eV. In particular, they take values of 0.3(3) eV for bulk, 0.2(5) eV in VP and 0.20(3) eV in AGC, thus suggesting a slight decreasing trend with increasing confinement. A NMR study[41] on the IL Emim-SCN confined in SiO_2 matrix with pores of similar size finds a contrary trend of the diffusion coefficients towards lower temperatures. There, the bulk dynamics are clearly faster than the confined dynamics. Only the detailed pore size variation between 59 and 82 Å obtains trends that appear unsystematic – so we would rather look on the average values for all studied pores. The obtained Arrhenius energies lie in the range of 0.3 eV, similar to ours. A much closer value using neutron backscattering spectroscopy on Bmim-PF_6 was found elsewhere[42]. About 10 times slower modes of the NMR study[41] are addressed to the near surface diffusion, a contribution with lower weight, which would appear in our study as the elastic line indistinguishable from the instrumental resolution. In Figure 4 c) the obtained diffusion constants follow the Arrhenius law quite well (with the number of points available). Typically, the main relaxation in glass forming substances, the α-relaxation, follows a non-Arrhenius behaviour. The phase behaviour of the ionic liquid bmim-PF_6 has been described in Ref.[31], where elastic fixed window scans (EFWS) with the backscattering spectrometer revealed that the IL can be strongly supercooled, or can crystallize, depending on the heating or cooling pathway. We conducted differential scanning calorimetry (DSC) measurements on the bulk liquid and elastic fixed window scans with the backscattering instrument obtaining information on the phase behaviour of EmimAc IL. Figure 5 shows the DSC results. A phase transition to a crystalline phase has been observed at 319 K upon cooling. Characteristics of a glass transition could be seen at or below 269 K (±10 K), with some limitation concerning the accessible temperature range in DSC. The EFWS experiment discussed in the next lines, which spans over a larger temperature range, will shed additional light onto the glass transition temperature. The crystallization corresponds to the for-

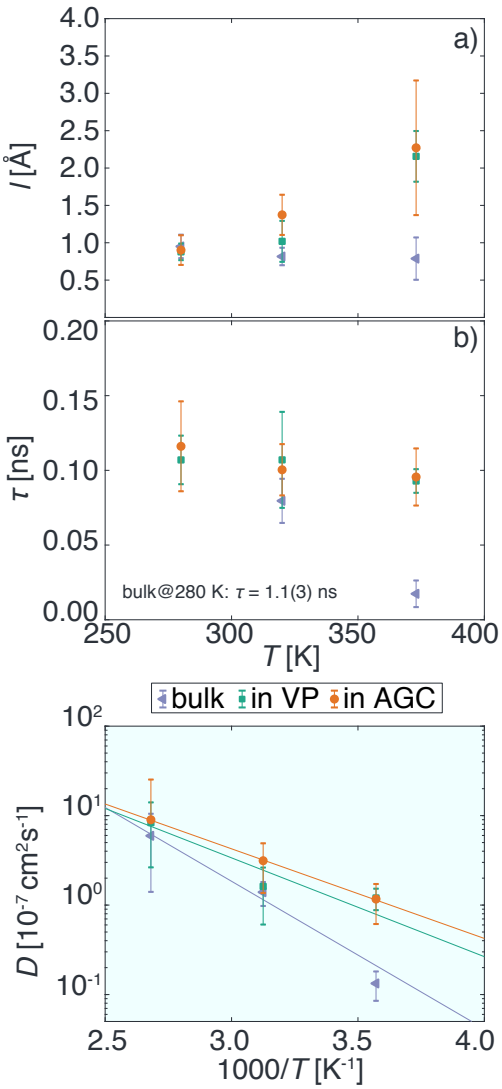

Fig. 4 a) Average jump lenght and b) residence time as obtained from the fits of Fig. 3. The τ value for the bulk at 280 K, not reported in the graph, is 1.0(3) ns. c) Arrhenius plot of the diffusion coefficient (solid lines represent fits according to Arrhenius equation).

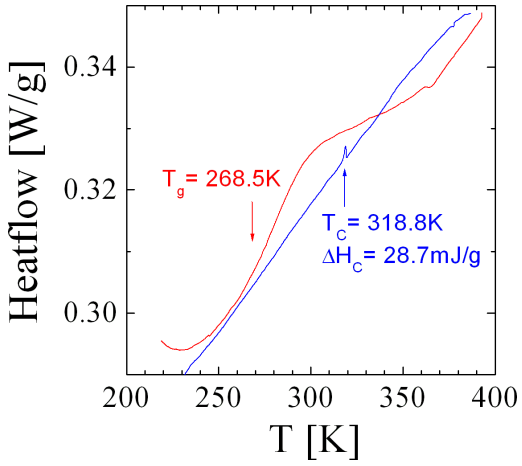

Fig. 5 Differential scanning calorimetry (the modulus of the heat flow) of the bulk EmimAc IL during heating (red) and cooling (blue) at 10 K/min. Crystallization into a lamellar phase is visible during the cooling at 319 K, and the signature of a glass transition at 269 K (±10 K) during the heating.

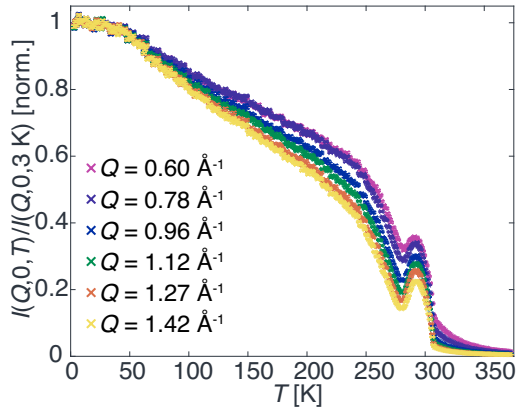

Fig. 6 EFWS for the bulk IL. The onset of the main relaxation process starts at around 260 K, when the mobility increases, a rearrangement into a crystalline (lamellar) phase takes place above 290 K. The larger temperatures of the QENS data have been therefore in the liquid phase.

mation of a lamellar structure in the IL. QENS experiments were conducted at three temperatures, where the two higher temperatures are in the liquid phase of the IL. We therefore think that our interpretation with the jump diffusion model is adequate. The lowest temperature is below the crystallization temperature, but above the glass transition temperature obtained from DSC. EFWS showed the onset of the main relaxation process above 240 K (Figure 6). There, also the crystallizing step approaching the crystallization temperature upon heating is clearly visible as a peak in the elastic intensity of the bulk IL. The crystallization starts at 280K, where the intensity begins to rise again with temperature. Above 310K the IL is molten and is in the liquid state. One might arrive in a supercooled liquid state when cooling from high temperatures across the crystallization temperature. The DSC measurements in Fig. 5 on the other hand indicate that also upon cooling some crystallization might take place. The scattered intensity below the „crystallization peak“ in the EFWS scans follows always the same curve, upon heating as well as upon cooling, only in the region of the crystallization peak deviations might occur. The DSC measurements and the elastic scans of the bulk EmimAc IL shows that the IL is liquid at the higher temperatures, for the lowest one further and more detailed studies are planned to shed light on the behaviour around the crystallization temperature into the lamellar phase and at lower temperatures.

The IL displays a clear capillary condensation[43] in both pores according to the XRD measurements that results from the attraction of cations to the glass surface, meaning that lamellar structures snuggle to the glass walls and fill in the whole volume. I.e. the preferential attraction of cations to the negatively charged glass walls (due to the dissociation of the silanol groups) leads to an onion-like domain alignment all over the volume. The center volume of mismatch inside each pore is clearly negligible for the scattering, however the ordered bulk structure is dominating the

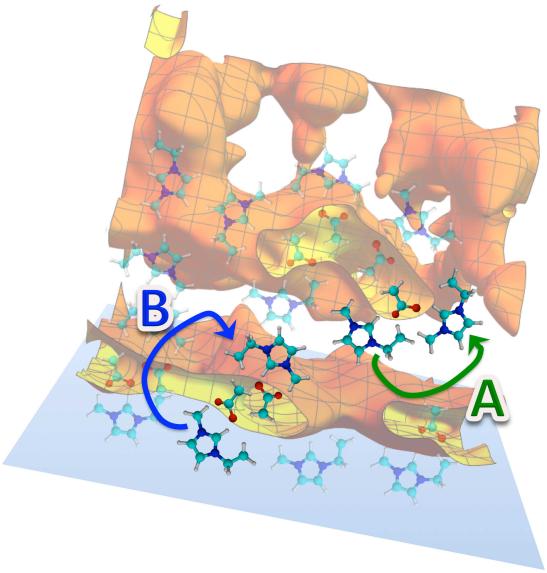

Fig. 7 Sketch of bicontinuous and lamellar domain structure in the bulk and at the glass wall (blue). The possible jumps in the bicontinuous bulk (A) and in the lamellar structure (B) are indicated. Please note, that the lamellar ordering is capillary condensed and not only a single layer at the glass wall.

results from scattering experiments. So, this situation clearly allows for several (10-25) domain spacings being placed inside the pores. In our "mild" confinement the correlation peak is therefore still prominent, with changes of the correlation length indicating the confinement effects (Fig. 1). In this sense, our situation describes an onset of confinement at an early stage, where an ordered bulk structure is formed and governs the results of our experiments. Contrarily to carbon nanotubes[17,18] and nanometer confinements in simulations[14,15], where also density mismatches may occur, the surface scattering from the 1-2 molecule layers would be dominating. Eventually, the static correlation peak would be lost in strong confinement[19].

When focusing on the dynamic parameters l and τ at the highest temperature of 373 K, both bulk values are clearly smaller than for the confined samples. When looking at the structural differences of the domains that are bicontinuous and lamellar (Fig. 7), the possible jumps in a bicontinuous structure can easily happen along the domain boundaries (case A) while in the lamellar structure the whole domain needs to be overcome (case B). For the overall diffusion, this different jump mechanism does not seem to play an important role, because two smaller values of l and τ nearly compensate each other. The absolute values of D are quite comparable. However, looking in more detail to the activation energies (in the sense of Arrhenius), the values decrease with confinement. Considering the much higher osmotic compressibility of the AGC sample, the distortion of the IL structure is so high that jumps seem to be facilitated, because the possible domain structure is far from the preferred equilibrium structure without confinement. A structural distortion has direct impact on the dynamic properties. However, our observed distortions are still relatively "mild" compared with other studies where the confinement allowed for only 1-2 molecule layers in between. Contrarily, in carbon nanotubes the acceleration of the diffusion can be dramatic[17,18]. Possibly, a density mismatch causes this effect.

When looking on the two lower temperatures, the parameter l is quite low in all cases indicating shorter jumps in the diffusion process. The translational diffusion characteristics in the bulk at low temperatures are also confirmed by QENS and MD simulations[44]. However, at lower temperatures the dynamical characteristics resemble more like the one from lamellar arrangements[33]. We believe that transient perforations with considerable residence times in the 'wrong' domain for the diffusing ions play a major role for all domain structures at lower temperatures because the slowing down of all motions captures the ions also in the transiting state. This goes along with smaller l-values. Whether the structure is bicontinuous or lamellar does not play a major role anymore. However, the confinement introduces distortions to the structure that keep the residence times much shorter than in the relaxed lamellar bulk phase.

4 Conclusions

Summarizing our study, the onset of confinement of the IL EmimAc in porous glasses was monitored in the very early stage, where the relation of changed domain structure and dynamics is visible. A connection between domain structure and a characteristically different jump diffusion mechanism was observed. Furthermore the onset of this "mild" confinement leads to a weak distortion of the lamellar domains, which reduces the activation energies of the jump diffusion. Future investigations are planned where molecular dynamics simulations shall be combined with neutron scattering experiments to get a deeper understanding of structural and dynamic changes under confinement at different temperatures. In particular, neutron spin echo measurements are planned to access longer timescales than the present one, in order to gather information on the slower dynamics.

Conflicts of interest

There are no conflicts to declare.

Acknowledgements

This work is based upon experiments performed at the instrument SPHERES operated by Jülich Centre for Neutron Science (JCNS) at the Heinz Maier-Leibnitz Zentrum (MLZ), Garching, Germany. We would like to acknowledge the support for the DSC measurements on a Mettler Toledo DSC 3 STARe System by Jia-Jhen Kang from Technische Universität München.

Notes and references

1 P. Wasserscheid and T. Welton, *Ionic liquids in synthesis*, John Wiley & Sons, 2008.
2 H. Ohno, *Electrochemical aspects of ionic liquids*, John Wiley & Sons, 2005.
3 B. Kirchner, in *Ionic Liquids*, vol. 290, pp. 1–345.
4 A. Triolo, O. Russina, U. Keiderling and J. Kohlbrecher, *The Journal of Physical Chemistry B*, 2006, **110**, 1513–1515.
5 R. D. Rogers and K. R. Seddon, *Science*, 2003, **302**, 792–793.
6 K. Wippermann, J. Wackerl, W. Lehnert, B. Huber and C. Ko-

rte, *Journal of The Electrochemical Society*, 2016, **163**, F25–F37.
7 M. Mezger, R. Roth, H. Schröder, P. Reichert, D. Pontoni and H. Reichert, *J. chem. phys.*, 2015, **142**, 164707.
8 H. Weiss, J. Mars, H. Li, G. Kircher, O. Ivanova, A. Feoktystov, O. Soltwedel, M. Bier and M. Mezger, *J. Phys. Chem. B*, 2017, **121**, 620–629.
9 K. Fujii, R. Kanzaki, T. Takamuku, Y. Kameda, S. Kohara, M. Kanakubo, M. Shibayama, S.-i. Ishiguro and Y. Umebayashi, *The Journal of chemical physics*, 2011, **135**, 244502.
10 C. Hardacre, J. D. Holbrey, C. L. Mullan, T. G. Youngs and D. T. Bowron, *The Journal of chemical physics*, 2010, **133**, 074510.
11 C. Patrascu, F. Gauffre, F. Nallet, R. Bordes, J. Oberdisse, N. de Lauth-Viguerie and C. Mingotaud, *ChemPhysChem*, 2006, **7**, 99–101.
12 T. I. Morrow and E. J. Maginn, *J. Phys. Chem. B*, 2002, **106**, 12807–12813.
13 K. Shimizu, M. Tariq, A. A. Freitas, A. A. Pádua and J. N. Lopes, *J. Braz. Chem. Soc.*, 2016, **27**, 349–362.
14 S. Mossa, *Phys. Rev. X*, 2018, **8**, 031062.
15 R. Futamura, T. Iiyama, Y. Takasaki, Y. Gogotsi, M. J. Biggs, M. Salanne, J. Segalini, P. Simon and K. Kaneko, *Nature materials*, 2017, **16**, 1225.
16 F. Ferdeghini, Q. Berrod, J.-M. Zanotti, P. Judeinstein, V. G. Sakai, O. Czakkel, P. Fouquet and D. Constantin, *Nanoscale*, 2017, **9**, 1901–1908.
17 Q. Berrod, F. Ferdeghini, P. Judeinstein, N. Genevaz, R. Ramos, A. Fournier, J. Dijon, J. Ollivier, S. Rols, D. Yu, R. A. Mole and J.-M. Zanotti, *Nanoscale*, 2016, **8**, 7845–7848.
18 S. Chathoth, E. Mamontov, S. Dai, X. Wang, P. Fulvio and D. Wesolowski, *EPL (Europhysics Letters)*, 2012, **97**, 66004.
19 B. Dyatkin, N. C. Osti, Y. Zhang, H.-W. Wang, E. Mamontov, W. T. Heller, P. Zhang, G. Rother, P. T. Cummings, D. J. Wesolowski *et al.*, *Carbon*, 2018, **129**, 104–118.
20 J. L. Bañuelos, G. Feng, P. F. Fulvio, S. Li, G. Rother, N. Arend, A. Faraone, S. Dai, P. T. Cummings and D. J. Wesolowski, *Carbon*, 2014, **78**, 415–427.
21 F. T. Kohler, B. Morain, A. Weiß, M. Laurin, J. Libuda, V. Wagner, B. U. Melcher, X. Wang, K. Meyer and P. Wasserscheid, *ChemPhysChem*, 2011, **12**, 3539–3546.
22 J. Viell, H. Inouye, N. K. Szekely, H. Frielinghaus, C. Marks, Y. Wang, N. Anders, A. C. Spiess and L. Makowski, *Biotechn. biofuels*, 2016, **9**, 7.
23 T. Sen and M. Barisik, *Scientific reports*, 2019, **9**, 137.
24 J. Wuttke, A. Budwig, M. Drochner, H. Kämmerling, F.-J. Kayser, H. Kleines, V. Ossovyi, L. C. Pardo, M. Prager, D. Richter *et al.*, *Rev. sci. instr.*, 2012, **83**, 075109.
25 J. Wuttke, *slaw*, `http://apps.jcns.fz-juelich.de/slaw`.
26 D. Richard, M. Ferrand and G. J. Kearley, *Journal of Neutron Research*, 1996, **4**, 33–39.
27 M. Teubner and R. Strey, *J. Chem. Phys.*, 1987, **87**, 3195–3200.
28 C. Frank, H. Frielinghaus, J. Allgaier and H. Prast, *Langmuir*, 2007, **23**, 6526–6535.
29 F. Nallet, D. Roux and S. Milner, *J. Physique*, 1990, **51**, 2333–2346.
30 T. Zemb, D. Gazeau, M. Dubois and T. Gulik-Krzywicki, *EPL (Europhys. Lett.)*, 1993, **21**, 759.
31 A. Triolo, O. Russina, V. Arrighi, F. Juranyi, S. Janssen and C. M. Gordon, *The Journal of chemical physics*, 2003, **119**, 8549–8557.
32 O. Russina, M. Beiner, C. Pappas, M. Russina, V. Arrighi, T. Unruh, C. L. Mullan, C. Hardacre and A. Triolo, *The Journal of Physical Chemistry B*, 2009, **113**, 8469–8474.
33 M. Kofu, M. Nagao, T. Ueki, Y. Kitazawa, Y. Nakamura, S. Sawamura, M. Watanabe and O. Yamamuro, *The Journal of Physical Chemistry B*, 2013, **117**, 2773–2781.
34 S. M. Chathoth, E. Mamontov, P. F. Fulvio, X. Wang, G. A. Baker, S. Dai and D. J. Wesolowski, *EPL (Europhysics Letters)*, 2013, **102**, 16004.
35 J. P. Embs, T. Burankova, E. Reichert and R. Hempelmann, *The Journal of Physical Chemistry B*, 2012, **116**, 13265–13271.
36 C. Cerclier, J.-M. Zanotti, J. Embs and J. Le Bideau, *Meeting Abstracts*, 2014, **MA2014-02**, 1418.
37 C. V. Cerclier, J.-M. Zanotti and J. L. Bideau, *Phys. Chem. Chem. Phys.*, 2015, **17**, 29707–29713.
38 S. Mitra, C. Cerclier, Q. Berrod, F. Ferdeghini, R. De Oliveira-Silva, P. Judeinstein, J. Le Bideau and J.-M. Zanotti, *Entropy*, 2017, **19**, year.
39 M. Bée, *Quasielastic Neutron Scattering: Principles and Applications in Solid State Chemistry, Biology and Materials Science*, Adam Hilger, Bristol and Philadelphia, 1988.
40 K. Singwi and A. Sjölander, *Phys. Rev.*, 1960, **119**, 863.
41 D. Kruk, M. Wojciechowski, Y. L. Verma, S. K. Chaurasia and R. K. Singh, *Physical Chemistry Chemical Physics*, 2017, **19**, 32605–32616.
42 A. Triolo, O. Russina, C. Hardacre, M. Nieuwenhuyzen, M. A. Gonzalez and H. Grimm, *The Journal of Physical Chemistry B*, 2005, **109**, 22061–22066.
43 M. Alibalazadeh and M. Foroutan, *Journal of molecular modeling*, 2015, **21**, 168.
44 B. Aoun, M. A. González, J. Ollivier, M. Russina, Z. Izaola, D. L. Price and M.-L. Saboungi, *The Journal of Physical Chemistry Letters*, 2010, **1**, 2503–2507.